Article

Direct Electrodeposition of CuSb for Lithium-Ion Battery Anodes

James M. Mosby, and Amy L. Prieto

J. Am. Chem. Soc., **2008**, 130 (32), 10656-10661 • DOI: 10.1021/ja801745n • Publication Date (Web): 16 July 2008

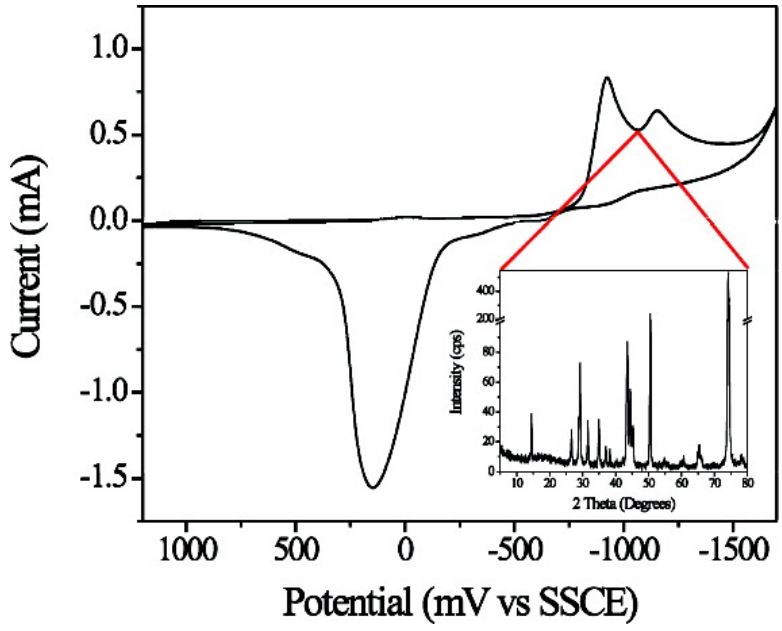

More About This Article

Additional resources and features associated with this article are available within the HTML version:

- Supporting Information
- Links to the 1 articles that cite this article, as of the time of this article download
- Access to high resolution figures
- Links to articles and content related to this article
- Copyright permission to reproduce figures and/or text from this article

View the Full Text HTML

J|A|C|S
ARTICLES

Published on Web 07/16/2008

Direct Electrodeposition of Cu_2Sb for Lithium-Ion Battery Anodes

James M. Mosby and Amy L. Prieto*

Department of Chemistry, Colorado State University, Fort Collins, Colorado 80523

Received March 9, 2008; E-mail: amy.prieto@colostate.edu

Abstract: We describe the direct single potential electrodeposition of crystalline Cu_2Sb, a promising anode material for lithium-ion batteries, from aqueous solutions at room temperature. The use of citric acid as a complexing agent increases the solubility of antimony salts and shifts the reduction potentials of copper and antimony toward each other, enabling the direct deposition of the intermetallic compound at pH 6. Electrodeposition of Cu_2Sb directly onto conducting substrates represents a facile synthetic method for the synthesis of high quality samples with excellent electrical contact to a substrate, which is critical for further battery testing.

Introduction

There is widespread interest in developing novel battery materials that can improve upon widely used rechargeable lithium-ion batteries. Currently, rechargeable lithium-ion batteries are the most popular choice to power portable electronics because of their high energy density and low weight.[1] Dendritic growth of metallic lithium onto the commonly used graphite anodes can lead to shorting in the battery and cause safety issues.[1] Therefore, new anode materials and morphologies[2] are desired in which these safety issues, as well as the capacity and the charge/discharge rates, can be improved over graphite. One group of materials that shows promise as alternatives to graphite are intermetallics.[3]

Intermetallic compounds have been investigated as alternatives to graphite because they offer the possibility of improved capacity, a highly reversible reaction with lithium, and a lithium intercalation potential that can be less negative than the deposition potential of metallic lithium.[3–7] The latter is critical for eliminating dendritic growth of elemental lithium on the electrode. The major drawback of using intermetallics as anode materials is the irreversible capacity loss during cycling due to large volume changes.[3] These large volume changes result in pulverization of the electrode during cycling and, consequently, a loss of electrical contact between the anode and the rest of the battery.

Cu_2Sb, however, is an intermetallic that does not exhibit these large volume changes during the charging and discharging.[8] Fransson et al. demonstrated that Cu_2Sb intercalates lithium to form Li_3Sb in a Cu matrix with relatively small volume changes and long cycle life, exhibiting a volumetric capacity of 1914 mAh/mL after 25 cycles.[4] The small volume change during cycling is attributed to the strong structural relationship between the lithiated and delithiated compound.[8] The antimony atoms are arranged in a face centered cubic array that acts as a flexible framework for lithium insertion during charging. Metallic copper is then extruded to the surface of each crystallite, which is proposed to create a conducting matrix that maintains electrical contact from grain to grain. Another benefit of Cu_2Sb is that its operating potential precludes lithium metal plating. While novel materials can improve the performance of batteries, changing the morphology of known materials can equally enhance their performance. Increasing the surface area of electrode materials has been shown to dramatically enhance the rate of lithium intercalation and extend cycle life.[2] To that end, we are interested in developing a synthetic method that will provide control over the composition, morphology, and surface area of Cu_2Sb anodes.

Current syntheses of Cu_2Sb include pulsed laser deposition, crystal growth from melts, ball milling, and chemical reduction from solution.[4–7,9,10] Some of these methods are plagued by high reaction temperatures which can cause Sb loss over time (because of its high vapor pressure relative to Cu) resulting in heterogeneous final products. The other synthetic strategies, including solution routes employing the addition of reducing agents to the reaction mixture, generally require postannealing. An exception to this was reported by Wan et al.[11] where sodium citrate was used as a complexing agent and potassium borohy-

(1) Tarascon, J.-M.; Armand, M. *Nature* **2001**, *414*, 359.
(2) Sides, C. R.; Li, N.; Patrissi, C. J.; Scrosati, B.; Martin, C. R. *MRS Bull.* **2002**, *27*, 604.
(3) Winter, M.; Besenhard, J. O. *Electrochim. Acta* **1999**, *45*, 31.
(4) Fransson, L. M. L.; Vaughey, J. T.; Benedek, R.; Edstrom, K.; Thomas, J. O.; Thackeray, M. M. *Electrochem. Commun.* **2001**, *3*, 317.
(5) Fransson, L. M. L.; Vaughey, J. T.; Edstrom, K.; Thackeray, M. M. *J. Electrochem. Soc.* **2003**, *150*, A86.
(6) Song, S. W.; Reade, R. P.; Cairns, E. J.; Vaughey, J. T.; Thackeray, M. M.; Striebel, K. A. *J. Electrochem. Soc.* **2004**, *151*, A1012.
(7) Sarakonsri, T.; Johnson, C. S.; Hackney, S. A.; Thackeray, M. M. *J. Power Sources* **2006**, *153*, 319.
(8) Thackeray, M. M.; Vaughey, J. T.; Johnson, C. S.; Kropf, A. J.; Benedek, R.; Fransson, L. M. L.; Edstrom, K. *J. Power Sources* **2003**, *113*, 124.
(9) Vitkina, T. Z.; Zhigadlo, N. D.; Ryzhkovskii, V. M. *Cryst. Res. Technol.* **1988**, *23* (7), 945.
(10) Kulifay, S. M. *J. Am. Chem. Soc.* **1961**, *83*, 4916.
(11) Ren, J.; He, X.; Pu, W.; Jiang, C.; Wan, C. *Electrochim. Acta* **2006**, *52*, 1538.

10.1021/ja801745n CCC: $40.75

dride as a reducing agent at pH 12, resulting in fine Cu_2Sb powders. All of the previously mentioned synthetic methods, except pulsed laser deposition, produce powders that must be suspended in binders in order to evaluate the materials' performance. Electrodeposition, however, is not plagued by these drawbacks.

The distinct advantage of the electrodeposition described here is that the active material (Cu_2Sb) is deposited directly onto a conducting substrate with excellent electrical contact without requiring postannealing. Electrodeposition also provides precise control of composition and thickness under mild conditions. In addition this method can be used to deposit on to complex shapes and into deep recesses.[12,13] Electrodeposition of intermetallics is complicated, however, by the requirement that the deposition potential and rates of at least two elements must be controlled simultaneously.[14–16] In particular, codeposition of Cu and Sb from aqueous solutions presents two challenges. The first is that the reduction potentials of Cu and Sb differ by approximately 130 mV in aqueous solutions, and the deposition of Cu is preferred at less negative potentials.[17] The second challenge in this system is that while antimony salts are soluble in acidic solutions, they precipitate in neutral aqueous solutions to form Sb_2O_3. The electrodeposition of Sb is not possible in acidic solutions because protons are reduced to H_2 at potentials less negative than what is required to reduce Sb^{3+}. It is therefore imperative to force Sb^{3+} to remain soluble in less acidic solutions and/or shift its reduction potential to less negative potentials.

We chose citric acid to keep Sb^{3+} in solution because of its history as a complexing agent in separate deposition solutions of copper and antimony.[18–20] The resulting complexation of the Sb^{3+} by the citrate species in solution allows the pH to be raised without the formation of Sb_2O_3, and results in a widening of the electrochemical window of the solution toward more negative potentials. This is critical for the direct deposition of our desired compound. Herein we report the direct electrodeposition of Cu_2Sb from aqueous solutions containing the required stoichiometric amount of copper versus antimony (for Cu_2Sb) and using citric acid as a complexing agent. Under the optimal conditions of pH and citric acid concentration *Cu metal cannot be deposited directly from solution without the presence of the Sb-citrate species.* This means that the solution chemistry of both metals complexed by citric acid is critical for the deposition of Cu_2Sb. The electrodeposition of Cu_2Sb was performed at room temperature and at a single potential onto copper substrates resulting in a Cu_2Sb thin film that is homogeneous, stoichiometric, and crystalline.

Experimental Section

Cu_2Sb films were electrodeposited from aqueous 0.4 M citric acid solutions (denoted H_3Cit, 99.5+% Aldrich) containing 0.025 M antimony(III) oxide (Sb_2O_3, nanopowder, 99.9+% Aldrich), and 0.1 M copper(II) nitrate hemipentahydrate ($Cu(NO_3)_2$, 99.9+% Aldrich). The solution was prepared by adding the citric acid to Millipore water (18 Ω) followed by the addition of Sb_2O_3. The dissolution of the Sb_2O_3 was aided by mechanical stirring. Upon complete dissolution, the $Cu(NO_3)_2$ was then added, turning the solution blue. The pH was subsequently raised to 6 by the addition of 5 M potassium hydroxide (KOH, ACS certified, Fisher) resulting in a dark blue solution. The optimal solution parameters were found by varying precursor concentrations and solution pH. The Cu_2Sb films were obtained by performing bulk electrolysis at room temperature and at a potential of −1050 mV versus a saturated sodium calomel electrode (SSCE). The temperature and the potential were also systematically varied to find the optimal deposition conditions.

The cyclic voltammograms (CVs) and depositions were conducted using a three-electrode cell and a BAS 100B potentiostat. Platinum gauze was used as a counter electrode, and a SSCE (0.236 V versus the standard hydrogen electrode) was used as the reference electrode. A platinum disk electrode (2.01 mm^2) or a glassy carbon electrode (7.0 mm^2) was used as the working electrode for the CVs, and copper or gold flag electrodes were used for the depositions. The copper flags were copper foil (0.25 mm thick, 99.98% Aldrich) with an area of 2−4 cm^2. The copper flags were mechanically polished using diamond paste and electrochemically polished in phosphoric acid (H_3PO_4, 85%, Mallinckrodt Chemicals) at a current of 0.15 A for less than 5 s. The gold substrates were made using a Denton vacuum evaporator with a Maxtek MDC-260 deposition controller. Approximately 10 nm of chromium were evaporated onto glass slides as an adhesion layer, followed by 300 nm of gold. Electrical contact was made by connecting a copper wire to the flag with carbon paint or an alligator clip. Clear nail polish was used to insulate the edges of the substrate and the back of the copper foil to ensure that deposition only occurred on flat surfaces with a controlled surface area. The depositions were carried out at a constant potential for 10 minute periods. The films were rinsed with Millipore water and allowed to air-dry.

Survey X-ray photoelectron spectroscopy (XPS) measurements were performed with a 5800 series Multi-Technique ESCA system and analyzed using Multipak software. An Al monochromatic source operating at 350.0 W was scanned from 10 to 1110 eV. XPS survey scans were taken before and after sputtering with an argon ion beam at 2 kV and a 3 × 3 raster. The sputtering removed a layer of adventitious carbon and any surface oxide that could have formed on the film during drying. High resolution XPS was performed using a signal-to-noise ratio of 300 for the Cu 2p and Sb 3d peaks. The powder X-ray diffraction (XRD) patterns were obtained using Cu Kα radiation from a Scintag X-2 Advanced Diffraction X-ray cabinet system that is equipped with a stationary stage and a Peltier detector. For the grain size calculations, the Scherrer technique was applied using DMSNT version 1.36b and CrystalliteSize version 1.01. The instrument peak broadening was determined via analysis of a SiO_2 standard. Scanning electron microscope (SEM) images of films were taken with a JEOL JSM-6500F equipped with an energy dispersive spectroscopy (EDS) detector from Thermo Electron. An accelerating voltage of 10 kV was used to image the films and collect EDS spectra.

Results and Discussion

Effect of pH on Deposition Potential. As mentioned previously, citric acid has been used widely in deposition solutions for both copper and antimony.[18–20] Because citric acid is a triprotic acid, solutions of varying pH were examined using cyclic voltammetry to study the effect of pH on the copper and antimony deposition potentials. Although this has already been done for the two elements separately, extensively for that of

(12) Switzer, J. A.; Shumsky, M. G.; Bohannan, E. W. *Science* **1999**, *284*, 293.
(13) Switzer, J. A.; Kothari, H. M.; Poizot, P.; Nakanishi, S.; Bohannan, E. W. *Nature* **2003**, *425*, 490.
(14) Sadana, Y. N.; Kumar, R. *Surf. Technol.* **1980**, *11*, 37.
(15) Saloniemi, H.; Kanniainen, T.; Ritala, M.; Leskelaae, M. *Thin Solid Films* **1998**, *326* (1−2), 78.
(16) Martin-Gonzalez, M.; Prieto, A. L.; Gronsky, R.; Sands, T.; Stacy, A. M. *J. Electrochem. Soc.* **2002**, *149*, C546.
(17) Lide, D. R. *The CRC Handbook of Chemistry and Physics*; CRC Press: Boca Raton, FL, 1999−2000; Vol. 80.
(18) Fouda, A. S.; Mohamed, A. K. *Bull. Electrochem.* **1990**, *6*, 677.
(19) Sadana, Y. N.; Kumar, R. *Plat. Surf. Finish.* **1979**, *66*, 58.
(20) Cattarin, S.; Furlanetto, F.; Musiani, M. M. *J. Electrochem. Soc.* **1994**, *24*, 439.

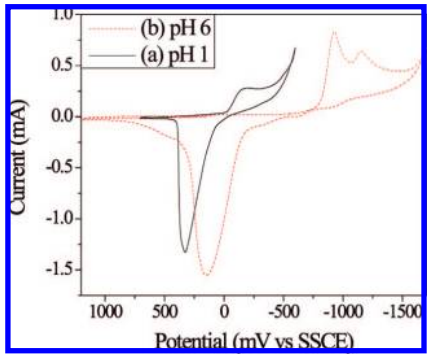

Figure 1. Cyclic voltammograms of 0.1 M $Cu(NO_3)_2$ and 0.025 M Sb_2O_3 (i.e., 0.05 M Sb^{3+}) in 0.4 M citric acid taken at (a) pH 1 and (b) pH 6. The reference electrode was a SSCE, the working electrode was Pt, and the scan rate was 250 mV/s.

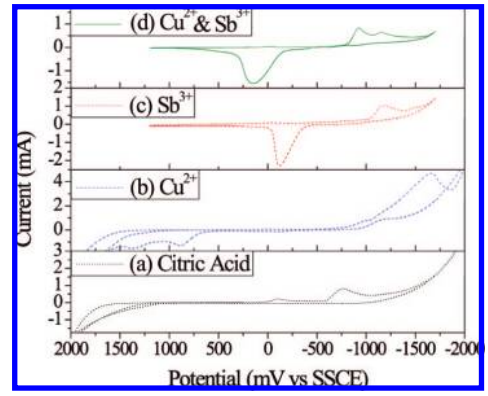

Figure 2. CVs of solutions containing (a) 0.4 M citric acid, (b) citric acid and 0.1 M $Cu(NO_3)_2$, (c) citric acid and 0.025 M Sb_2O_3, and (d) both metal precursors and citric acid. All solutions were at pH 6. A SSCE reference electrode and a Pt working electrode were used, and the scan rate was 250 mV/s.

copper[21–23] and in highly acidic solutions for that of antimony;[20,24] we are not aware of any reports of the electrochemistry of these two elements studied together in citrate solutions. Solutions containing $Cu(NO_3)_2$, Sb_2O_3, and citric acid were made ranging from pH 1 to pH 8. For these experiments, the concentrations of Cu^{2+} and Sb^{3+} were 0.1 and 0.05 M, respectively (before the addition of KOH). Examples of the CVs obtained are shown in Figure 1 for the pH 1 and 6 solutions (see Supporting Information Figure S1 for CVs taken from pH 1 to pH 8 inclusively).

The cathodic peak corresponding to the deposition of copper is clearly seen at −200 mV in Figure 1a. As the potential becomes more negative, the current increases rapidly due to the evolution of H_2 starting at approximately −460 mV. The assignment of the reduction peak at −200 mV was made because of its close match to the reduction peak in a CV of copper nitrate alone in citrate solutions at a similar pH. In contrast, the cathodic peak for the deposition of antimony cannot be seen at pH 1 because of the evolution of H_2; no stripping peak is observed. This suggests that under these conditions no antimony was deposited onto the working electrode because the electrochemical window of this solution is limited. The pH was then raised to eliminate H_2 evolution so that Sb could be electrodeposited.

In addition to significantly increasing the electrochemical window of the solution, raising the pH also controls which citrate species are present. Whereas at pH 1 the predominant species present for the citrate is the fully protonated species (denoted H_3Cit), at pH 6 there is a mixture of $HCit^{2-}$ and Cit^{3-}. Consequently, one can expect that the metal-ion binding at the different pHs will be different and could thereby shift the reduction potentials. Proof of this shift is evident in Figure 1. Once the electrochemical window is extended toward more negative potentials, the difference between the reduction potentials of the metal species in solution becomes smaller with increasing pH (Figure S1). At pH 6 this difference is the smallest, which is attractive because slightly acidic pH conditions preclude oxide precipitation during film deposition. We have assigned the small peak present at −118 mV in Figure 1b and Figure 2a (more clearly seen in Figure S2) to a surface phenomenon occurring on the Pt working electrode. This feature is not present in CVs run with a glassy carbon working electrode (see Figure S2). The CV of the pH 6 solution in Figure 1b exhibits a large cathodic peak at −950 mV, which can be attributed to the reduction of a copper citrate dimer (to be discussed shortly), followed by a shoulder located at −1150 mV corresponding to the reduction of Sb^{3+}. We assign these on the basis of a comparison of the CV of the deposition solution (Figure 2d) to CVs of the citrate solutions containing only citric acid (Figure 2a), each metal individually (Figure 2b,c), and from analysis of films deposited between −800 and −1200 mV.

The CV of citric acid alone exhibits two reduction peaks; one due to a surface phenomenon on Pt (at −118 mV) and one (at −750 mV) due to the reduction of a citrate species. As the pH is increased from 1 to 6 the CVs of each metal individually indicate that the Cu^{2+} reduction peak shifts in the negative direction while the Sb^{3+} reduction peak shifts in the positive direction. Deposition at a single potential (−1050 mV) results in the formation of Cu_2Sb. Upon switching the scan direction, a large oxidation peak is observed at 125 mV, corresponding to the stripping of Cu_2Sb. Only a single oxidation peak is observed, indicating that there is primarily a single oxidation process occurring at this potential. At much slower scan rates (10−50 mV/s, Figure S3) there is no change to the reduction peaks but there is a small shoulder to the main stripping peak; we are currently pursuing experiments to determine the effect of scan rate on this stripping peak.

Analysis of the two metals individually (Figure 2b,c) shows clear differences. The copper citrate solutions are complex because there are many different species present. When excess citrate is present, the two predominant copper−citrate species are dimers, both involving two copper and two citrate ions [$(Cu_2Cit_2H_{-2})^{4-}$ and $(Cu_2Cit_2H_{-1})^{3-}$].[21] The predominant species at pH 6 is $(Cu_2Cit_2H_{-2})^{4-}$, indicating that the smaller cathodic peak seen at −950 mV (Figure 2b) is likely due to the reduction of Cu^{2+} in the minority $(Cu_2Cit_2H_{-1})^{3-}$ species. This peak is at a similar potential as the first reduction peak seen in the deposition solution (Figure 3c,d). Copper electroreduction is significantly inhibited when $(Cu_2Cit_2H_{-2})^{4-}$ is the predominant species in solution, consistent with the absence of a stripping peak due to copper metal in Figure 2b.[22] To confirm this, constant potential experiments were performed in this solution at potentials more negative than −1250 mV. We

(21) Rode, S.; Henninot, C.; Vallieres, C. C.; Matlosz, M. *J. Electrochem. Soc.* **2004**, *151* (6), C405.
(22) Uksene, V.; Survila, A.; Zukauskaite, A. *Russ. J. Electrochem.* **1996**, *32*, 884.
(23) Gonzalez, S.; Alvarez, S. V.; Arevalo, A. *Electrochem. Acta* **1983**, *28*, 535.
(24) Sadana, Y. N.; Breau, J. G.; Du, N. *Metal Finish.* **1993**, *91*, 57.

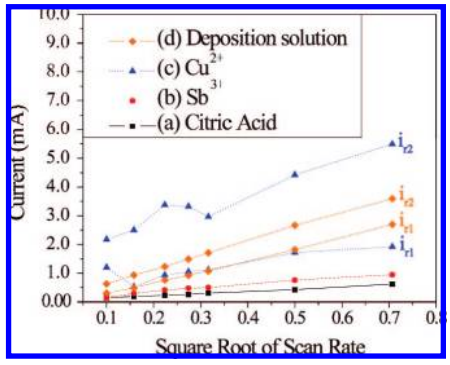

Figure 3. Current of the reduction peaks plotted versus square root of scan rate from solutions of (a) 0.4 M citric acid, (b) citric acid and 0.025 M Sb_2O_3, (c) citric acid and 0.1 M $Cu(NO_3)_2$, and (d) both metal precursors and citric acid. The i_{r1} and i_{r2} correspond to the current of the first reduction peak and second reduction peak of the CVs. All solutions were at pH 6. A SSCE reference electrode and a Pt working electrode were used.

observed no evidence of Cu metal on the working electrode. Consequently the last reduction peak at −1650 mV in Figure 2b is assigned to the reduction of $(Cu_2Cit_2H_{-2})^{4-}$ leading to the formation of the dimer complex $(Cu_2Cit_2(OH)_2)^{4-}$.[21,23] The absence of this reduction peak in Figure 2d indicates that the reduction of the dimer $(Cu_2Cit_2H_{-2})^{4-}$ does not occur in solutions that also contain antimony citrate. Under our conditions, it is evident that *copper metal is not deposited when Cu^{2+}alone is complexed by citrate at pH 6*. However, in the presence of antimony citrate we see two reduction peaks resulting in the deposition of Cu_2Sb.

Unlike the copper case, the electrochemistry of the antimony citrate solutions was found to be more straighforward even though there is a general lack of experimental data on the speciation present in antimony citrate solutions.[25] As mentioned previously, the reduction of Sb^{3+} in the citrate solution at pH 6 is observed at −1125 mV (Figure 2c). Two processes are occurring simultaneously at pH 6 resulting in the reduction of Sb^{3+} to Sb metal. The first is that with increasing pH the reduction peak for Sb^{3+} is shifted to more positive potentials. The second is that H_2 evolution is not a competing reaction at this pH, resulting in a larger electrochemical window, which includes potentials more negative than the Sb^{3+} reduction peak.

To further support the assignments made, we plotted the current of the reduction peaks for the different solutions at pH 6 versus the square root of the scan rate, as shown in Figure 3. Two important trends are clear. First, the current for the reduction peak of the solution containing only citric acid (Figure 3a) is the lowest of all the reduction peaks, even though citric acid is present at the highest concentration. Second, the current of the first reduction peak of the copper citrate solution (Figure 3b) and the deposition solution (Figure 3d) are similar. This indicates that the largest reduction peak in the deposition solution (Figure 3d) is due to a reduction process involving Cu^{2+} in the $(Cu_2Cit_2H_{-1})^{3-}$ species. As discussed above, the reduction of the $(Cu_2Cit_2H_{-2})^{4-}$ is not observed owing to the presence of antimony in solution.

On the basis of the data just described, we propose that Cu_2Sb is deposited directly at a single potential according to a simple coreduction mechanism.

$$2[Cu_2Cit_2H_{-1}]^{3-} + 2[SbCitH_{-1}]^{-} + 4H_3O^{+} + 14e^{-} \rightarrow 2Cu_2Sb + 6Cit^{3-} + 4H_2O.$$

This reaction accounts for the formation of the final product from slightly acidic solutions, keeping in mind the likely speciation present for the citrate ion. Although there is precedence for a single bimetallic Cu/Sb species in the solid state,[26] we have no evidence yet for the presence of such a species in solution under our conditions. Current work is focused on characterizing the speciation present under the optimal deposition parameters. Furthermore, deposition from a single bimetallic species would imply that the composition of the films would be constant regardless of potential. We will show that Cu_2Sb can be deposited at a range of potentials; however, the composition of the film changes from Cu-rich to Sb-rich as a function of increasingly negative potentials. This is consistent with the codeposition of two separate species, as noted in the reaction described above.

Effect of Citric Acid Concentration on Deposition. The optimal concentration of citric acid for the deposition solution was determined by varying the concentration between 0.2 and 0.8 M, in solutions containing 0.05 M Sb^{3+} and 0.1 M Cu^{2+}, separately. As the concentration of citric acid was increased, the current of the copper cathodic peak decreased. This can be attributed to the equilibrium of the copper citrate complexes; that is, as more citric acid is added, the availability of free copper ions in solution decreases. No difference in the anodic or cathodic current was observed for the antimony solutions, although enough citric acid needs to be present to complex all the antimony in order to prevent the precipitation of Sb_2O_3. The lower limit of citric acid needed to avoid the precipitation of Sb_2O_3, forming 0.05 M Sb^{3+} solutions, was found to be 0.4 M. Because lower concentrations of citric acid are desired for the copper deposition and at least 0.4 M citric acid is needed to keep Sb^{3+} in solution, 0.4 M citric acid was determined to be the optimal concentration. With these considerations in mind, all solutions used for subsequent experiments discussed contain 0.1 M $Cu(NO_3)_2$, 0.025 M Sb_2O_3, and 0.4 M citric acid adjusted to pH 6.

Effect of Deposition Potential and Temperature on the Film Composition. Using the optimal solution conditions found above, a systematic investigation of the deposition parameters was conducted. Films were deposited at different potentials surrounding the cathodic peaks seen in the CV shown in Figure 1b. The five potentials chosen were −800 (the onset of the first cathodic peak), −900, −1000 (the first peak maximum), −1100 (the onset of the second peak), and −1200 mV. Compositional results determined by XPS survey scans are contained in Table 1 and show that the ratio of Cu/Sb decreased with more negative

Table 1. XPS Data of Films Deposited at Different Potentials from Solutions Containing 0.1 M $Cu(NO_3)_2$, 0.025 M Sb_2O_3, and 0.4 M Citric Acid at pH 6[a]

potential mV vs SSCE	Cu 2p atomic %	Sb 3d atomic %
−800	76	24
−900	74	26
−1000	68	32
−1100	66	34
−1200	63	37

[a] In all cases the films were sputtered for 1 minute.

(25) Das, R.; Pani, S. *J. Indian Chem. Soc.* **1955**, *32*, 537.
(26) Smith, G.; Sagatys, D. S.; Bott, R. C.; Lynch, D. E. *Polyhedron* **1992**, *11*, 631.

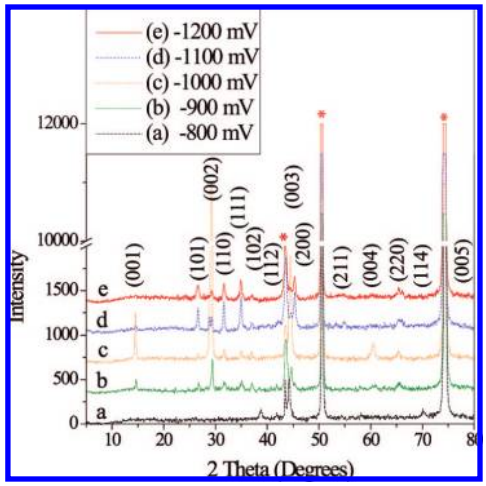

Figure 4. Powder XRD patterns of films deposited at different potentials using solutions containing 0.1 M $Cu(NO_3)_2$, 0.025 M Sb_2O_3, and 0.4 M citric acid at pH 6. Peaks due to the copper substrate are denoted with red asterisks, and peaks due to Cu_2Sb are indexed to PDF 85-492.

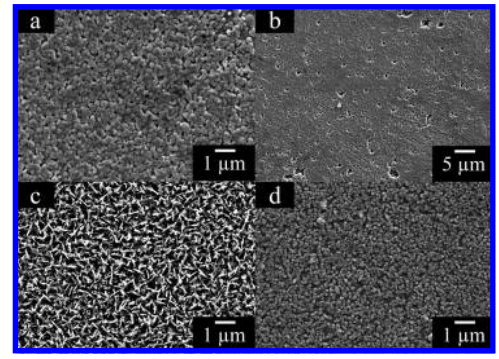

Figure 5. SEM images of films deposited at different potentials. The films were deposited at (a) −900, (b) −1000, (c) −1100, and (d) −1200 mV versus SSCE. The pH 6 deposition solution contained 0.1 M $Cu(NO_3)_2$, 0.025 M Sb_2O_3, and 0.4 M citric acid.

potentials (see Figure S4 for a typical XPS spectrum).[27] The qualitative trend is clear: relative to the desired 2/1 copper/antimony ratio, copper-rich films are deposited at less negative potentials and antimony-rich films are deposited at more negative potentials. The desired ratio was found for films deposited between −1000 and −1100 mV. This same trend was also observed in corresponding EDS data.

This trend in composition is consistent with the reaction described above. At less negative potentials (before the onset of the first peak observed in Figure 1 at pH 6), the reduction of $[Cu_2Cit_2H_{-1}]^{3-}$ should occur first. Since copper metal cannot be deposited from solutions of just $[Cu_2Cit_2H_{-1}]^{3-}$, there must be some interaction with the antimony species present which leads to a codeposition of the two elements. At more negative potentials the reduction of the antimony species dominates, resulting in Sb-rich films.

X-Ray diffraction (XRD) patterns, shown in Figure 4, were used for phase identification of the films deposited at the potentials listed in Table 1. The Cu substrate is responsible for the high intensity of the three peaks at 43, 50, and 74° 2θ, indexed to the copper (111), (200), and (220) reflections (PDF 04-836). Three additional peaks are observed in the XRD pattern of the film deposited at −800 mV (Figure 4a). All three of these peaks match peaks for Cu_2Sb (PDF 85-492), one of which is generally used as the fingerprint for the desired compound (the broad (003) peak at 44° 2θ). The absence of additional Cu_2Sb peaks and the copper-rich composition determined by XPS indicate that this film is at best a mixture of Cu, Cu_2Sb, Sb, and/or a solid solution of Cu and Sb. Multiple Cu_2Sb peaks (Miller indices for each reflection are shown) appear in the XRD patterns of the films deposited at all other potentials, indicating more crystalline films. The XRD patterns of the films deposited at −900 and −1000 mV (Figure 4b,c) are similar, but the peaks of the film deposited at −1000 mV have higher relative peak intensities than the film deposited at −900 mV. Note that all films were deposited for the same amount of time, so the increased peak intensities could be due to increased crystallinity or simply greater growth rate. Although the SEM images of these films also show similar surface morphologies, the film deposited at −900 mV (Figure 5a) shows larger features than the film deposited at −1000 mV (Figure 5b). The grain sizes of the film deposited at −1000 mV is also smaller than the film deposited at −900 mV. As calculated by the Scherer method, the film grown at −900 mV is composed of grains that have an average size of 90 nm, while the average size of the grains of the film deposited at −1000 mV is 35 nm.

The morphologies of the films deposited at −1100 and −1200 mV are consistent with the differences between their XRD patterns (Figure 4 panels c and d) and those of the films deposited at −900 and −1000 mV (Figure 4 panels a and b). The SEM image of the film deposited at −1100 mV (Figure 5c) clearly shows dendritic growth. The observed diameter of the rods was found to range from 50 to 150 nm with lengths greater than 600 nm. The average particle size calculated from peak broadening was 50 nm, corresponding to the smallest observed diameter from SEM. The SEM image of the film deposited at −1200 mV (Figure 5d) shows small spherical particles (200 nm) on the surface of the film with a calculated grain size less than 20 nm. XRD patterns of films deposited from −1100 to −1200 mV can be indexed using PDF 85-492 for Cu_2Sb and also have the predicted relative intensities. In addition, preferred orientation is apparently a function of deposition potential: films deposited at potentials more negative than −1100 mV are (111) versus the films deposited at −900 and −1000 mV, which exhibit (001) preferred orientation.

The effect of temperature on the electrodeposition of Cu_2Sb was also investigated. No differences in film composition were detectable by means of XPS for films deposited from 5 to 60 °C. The broadness of the XRD peaks decreased with increasing temperature (see Figure S5). Also, the surface morphology of Cu_2Sb films deposited at 60 °C exhibited cubic faceting (see Figure S6).

Cu_2Sb Films. On the basis of the previous observations, films of Cu_2Sb were deposited at room temperature in solutions of 0.4 M citric acid at a pH of 6 with 0.1 M $Cu(NO_3)_2$ and 0.025 M Sb_2O_3 at −1050 mV versus SSCE. Although the successful electrodeposition of Cu_2Sb was confirmed by the match of the films' XRD pattern to the peak positions of Cu_2Sb (PDF 85-492), three very small peaks at 38, 40, and 42° 2θ (circled in Figure 6) were observed. Each one of these reflections separately matches reflections of different oxides ($CuSb_2O_6$, Sb_2O_3, and CuO). We are hesitant, however, to identify the presence of any of these oxide phases on the basis of a single low-intensity reflection in an XRD pattern. In an effort to probe for the

(27) We have only shown two significant figures because our samples were not cleaved under high vacuum or run against a rigorous standard, as needed to obtain truly quantitative XPS data.

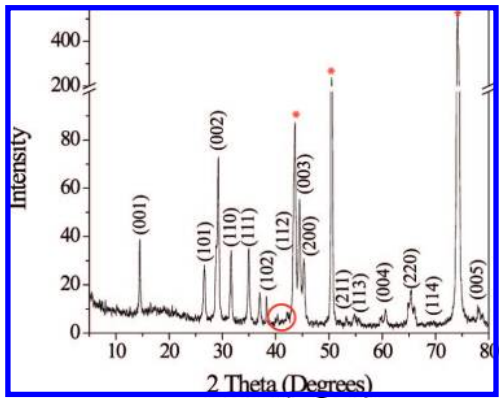

Figure 6. Powder XRD pattern of Cu_2Sb film deposited using optimized deposition solution and conditions. The peaks indicated by asterisks are from the Cu substrate, and peaks due to Cu_2Sb are indexed to PDF 85-492. The red circle surrounds the three peaks that do not index to Cu_2Sb.

presence of oxide phases or amorphous inhomogeneities in the as-deposited films, the film for which the XRD pattern is shown in Figure 6 was annealed for 5 h under argon at 220 °C (XRD pattern shown in S7). The peak positions observed in both XRD patterns match except the extra peaks seen in Figure 6 are not present after annealing, consistent with the removal of surface oxide phases.

All films discussed thus far were deposited in ten-minute periods from unstirred solutions. The film in Figure 6 has a thickness of 32.4 μm as determined by SEM on a cross-sectional image, and shows no signs of discontinuities or pores in a cross-sectional view of the film. Excluding any nucleation time, this corresponds to an average deposition rate of 3.24 μm per minute, compared to an average of 0.72 μm per minute for the deposition of copper from a 0.2 M $CuSO_4$ solution at a constant current of 10 mA.[28] The rapid growth rate that we observe indicates that the solution parameters or interaction of the metal precursors with the substrate may facilitate the electrodeposition of Cu_2Sb.

(28) Wu, A.; Barkey, D. P. *J. Electrochem. Soc.* **2003**, *150*, C533.

To determine the importance of the substrate, films were also deposited on gold substrates. For these films the same solution parameters and deposition conditions were used. The film deposited on Au was slightly less crystalline than the film deposited on Cu, but still exhibited a (001) preferred orientation (see Figure S8). This implies that the observed preferred orientation for films deposited at −1050 mV is not due to templating by the substrate. Hence we are confident that the solution chemistry in this case is critical for the observed deposition of crystalline Cu_2Sb.

Conclusions

We have developed a method for the direct electrodeposition of crystalline Cu_2Sb from aqueous solutions at room temperature using citric acid as a complexing agent. The pH was raised using KOH solutions, thereby increasing the electrochemical window of the solution toward more negative potentials. We observe that at a pH of 6, the reduction potentials of the copper and antimony species converge, resulting in the single potential deposition of Cu_2Sb. The solution chemistry of this system is critical for the deposition of the desired compound. The films deposited under these conditions are ideal for battery testing because they are crystalline, stoichiometric, and have excellent electrical contact to the substrates. Battery testing experiments on these samples are currently underway.

Acknowledgment. We thank Prof. C. M. Elliott for the use of the potentiostat in his laboratory and for extremely helpful discussions. We also thank Drs. Pat McCurdy and Sandeep Kohli (Central Instrument Facility) for assistance with the SEM, XPS, and XRD. This work was supported by funds from Colorado State University and the National Science Foundation Active Nanostructures program (Grant ECCS-0709412).

Supporting Information Available: Additional CVs, XRDs, SEMs. This material is available free of charge via the Internet at http://pubs.acs.org.

JA801745N